ACS OMEGA

Open Access

http://pubs.acs.org/journal/acsodf

Article

Harvesting Renewable Energy from Saltworks Waste Brines via Reverse Electrodialysis

Syed Abdullah Shah, Enrica Fontananova, Andrea Cipollina, Alessandro Tamburini,* Alberto Figoli, and Giorgio Micale

Cite This: *ACS Omega* 2025, 10, 29980−29991

Read Online

ACCESS | Metrics & More | Article Recommendations

ABSTRACT: The present work presents an experimental campaign devoted to producing electric power from waste brines with a laboratory-scale reverse electrodialysis (RED) unit. In particular, two saltworks waste brines (i.e., Margi and Nubia basins in Trapani, Italy) were used as feeds. Two different homogeneous ion exchange membranes (IEMs), developed by (I) Fujifilm Manufacturing Europe BV (The Netherlands) and (II) Suez (France), were investigated under several experimental conditions. Membrane ion sorption, fixed charge concentration, and permselectivity were investigated. Both real/pretreated brine and artificial solutions (5 M NaCl comparable to sodium chloride concentration in real brine) were investigated as feed solutions at 30 °C. Fujifilm IEMs resulted in higher stack permselectivity and yet exhibited higher resistance compared to Suez membranes. Monovalent ion sorption and counterion concentration of Fujifilm IEMs were higher than those of Suez membranes, while the co-ion concentrations in both IEMs were comparable. The RED application with hypersaline Margi-A and Nubia-A brine (TDS; 364.60 and 359.28 g/L) showed power densities of 3.57 and 4.32 W/m^2 for Fujifilm IEMs, respectively. Conversely, Suez IEMs provided significantly lower power densities of 0.77 and 0.69 W/m^2, respectively.

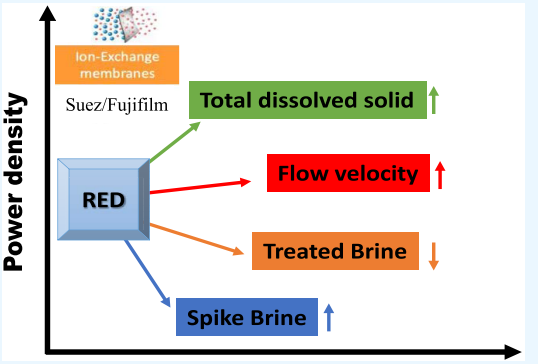

1. INTRODUCTION

According to the US Energy Information Administration, total worldwide power production is predicted to grow from 20 trillion to above 40 trillion kWh by 2040; among all energy sources currently rising in demand, renewable energy is the fastest growing by 2.8% ramp up per year.[1] The shift toward renewable energy sources and more efficient power generation methods substantially reduces greenhouse gas emissions and other pollutants. Salinity gradient power (SGP) is a novel blue energy source due to its architectural and technological advancement. SGP was originally proposed by Pattle in 1954 by mixing seawater and river water.[2] SGP has tremendous potential to meet global energy necessities, and the overall evaluated technical natural salinity potential energy is 647 GW, which corresponds to 23% of the global power consumption.[3,4] Suitable SGP application sites are estuaries where river water (freshwater) meets into the seawater,[5−7] saltworks and salt mining,[8,9] hypersaline stream from the desalination plant,[10,11] and saltwater lakes.[12]

The most promising membrane-based technologies for SGP harvesting are reverse electrodialysis (RED)[5,13] and pressure-retarded osmosis (PRO)[14,15] compared to other techniques.[16,17] Usually, a RED stack consists of alternating cation exchange membranes (CEMs) and anion exchange membranes (AEMs) between the cathode and anode, as described in Figure 1. The ion exchange membranes (IEMs) are kept apart from one another by placing a spacer in between. The resulting channels host feed saline. During the process, the ions move through the IEMs from the high-concentration compartment (HCC) to the low-concentration compartment (LCC) due to the salinity difference across the membranes. This ion flux is converted into electricity in electrodic channels via suitable reversible redox reactions occurring on the electrode surface when the external load resistance is connected to the circuit.[13]

In the framework of the SEArcularMINE project, which is focused on the sustainable valorization of brine for valuable mineral recovery and the harnessing of renewable energy through innovative technologies, a strategic approach has been implemented to address the complexities associated with divalent ions during the operation of a reverse electrodialysis (RED) system. The idea is that of removing divalent ions as magnesium ones upstream of the RED unit. Specifically, the RED unit has been fed with both untreated brine and brine

Received: September 20, 2024
Revised: October 28, 2024
Accepted: November 22, 2024
Published: July 8, 2025

https://doi.org/10.1021/acsomega.4c08651
ACS Omega 2025, 10, 29980−29991

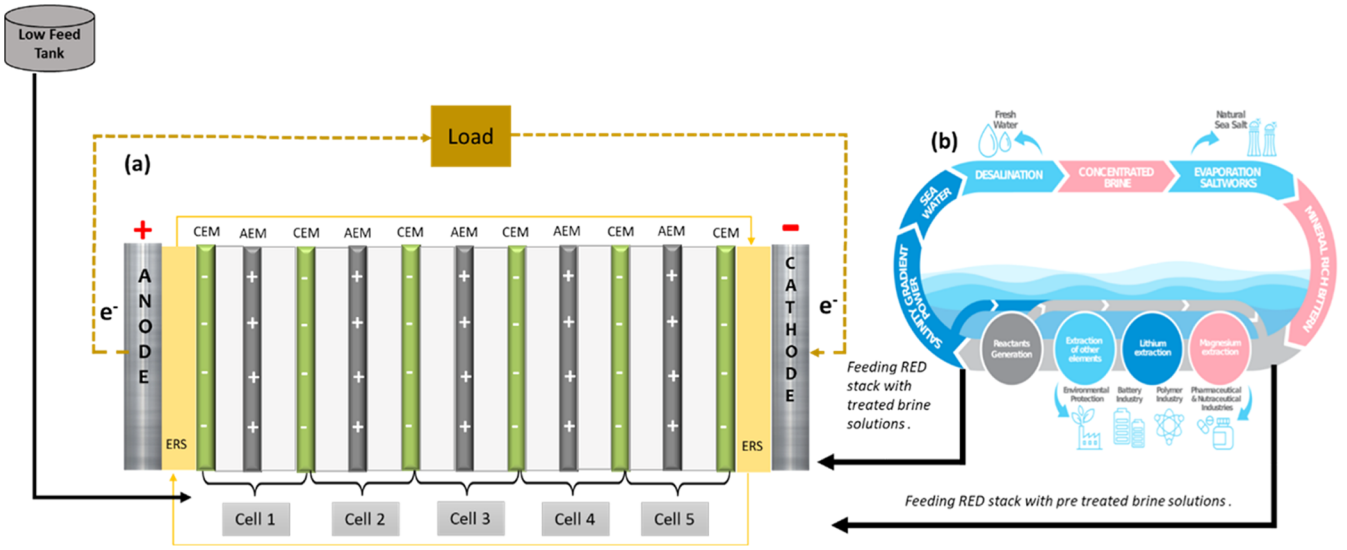

Figure 1. (a) Schematic representation of the reverse electrodialysis (RED) and (b) the SEArcularMINE project process.[19] CEM: cation exchange membrane; AEM: anion exchange membrane; ERS: electrode rinse solution.

that has undergone a treatment process within a magnesium hydroxide crystallization reactor (Mg-CGCR).[18] This innovative approach is poised to revolutionize the field by mitigating the impact of divalent ions, thereby enhancing the efficiency and effectiveness of the RED unit within the broader objectives of the SEArcularMINE project.[19]

The most widely available natural sources of salinity gradients are seawater and river water. In an ideal situation, the theoretically calculated SGP is very high, e.g., 1 m^3 seawater (30 kg m^{-3}) completely mixed with the same amount of river water (pure water) generates 1.7 MJ energy at 298 K, which can increase up to 6.1 MJ by a pure water/seawater volumetric ratio of 10:1.[20] By R.E Pattel in 1954, a power density of 0.20 W/m^2 was first determined via RED.[2] Currently, significant breakthroughs in membrane technology and membrane engineering have led to a rise in power density. RED units equipped with commercially available IEMs have shown maximum power densities of 6.7 and 12 W/m^2 in a laboratory-scale experimental study.[21,22] Kim et al. developed lab-scale pore-filling IEMs and obtained a power density of 2.4 W/m^2[23] The same author reported that the resistance of homemade IEMs was lower than that of commercially available IEMs such as AMX/CMX (Tokuyama Co., Japan), FAS/FKS (Fumatch GmbH, Germany), and AMV/CMV (Asahi Glass Co. Ltd., Japan). Choi et al. studied the effect of the ion exchange capacity of lab-made membranes in RED and reported a maximum power density of 0.69 W/m^2 using a single-cell pair RED stack.[24] Shah et al. observed 27 mW/m^2 maximum power density by a modified Nafion nanocomposite membrane (CEM) combined with FAA3 (AEM) at a 75 mL/min flow rate in a single-cell pair RED unit.[5] All of these studies focused on river−water−seawater, while very few efforts have been devoted to the investigation of multi-ion feed streams at higher concentrations (i.e., brines).

The aforementioned literature studies are carried out using only NaCl as a feed solution in the RED process. However, a diverse spectrum of monovalent and multivalent ions is available in the natural feed stream. The presence of divalent ions, such as (Ca^{2+}, Mg^{2+}, and SO_4^{-2}) in natural seawater and river water applications has been studied through experiments: the gross power density of the process was affected by multi-ion solutions compared to artificial NaCl solutions.[3,25] The most notable effects of the presence of divalent ions included an increase in IEM resistance, uphill transport, and a decrease in the Nernst potential. Avci et al. reported a power density of 0.46 W/m^2 and a stack resistance of 30.5 Ω using a natural feed solution at 60 °C, whereas an artificial feed solution at the same temperature indicated a power density of 1.41 W/m^2 and a stack resistance of 12.8 Ω.[3] Seawater reverse osmosis (SWRO) concentrate effluents yield a power density of 3.6−3.7 W/m^2 per cell pair in the RED unit.[26] Simões et al. operated a RED unit for 1 month with natural water at the Afsluitdijk, The Netherlands, and measured the gross power density between 0.3 and 0.4 W/m^2.[27] Cosenza et al. conducted a 25-day test of a RED unit using effluents from crude oil extraction processes. They achieved a maximum power density of 2.5 W/m^{-2} cP.[28] The power generation performance of a bench-scale RED stack (40 m^2) was evaluated using natural seawater RO brine and natural municipal wastewater as feed solutions. The study reported power densities of 0.41 and 0.54 W/m^2, with a maximum power output of 21.7 W.[29]

With this respect, the analysis of natural feed solutions discharged from saltworks is essential for a comprehensive comprehension of RED potential.

In this study, we investigated two distinct types of commercial membranes (Fujifilm and Suez), focusing on the effect of the counterions and co-ions relative to fixed charge groups. These ion exchange membranes were sourced from manufacturers and subjected to desorption techniques.

The membranes were equilibrated by exposure to external solutions containing NaCl (0.5, 1, and 5 M) and real Margi brine solutions. Additionally, we explored the permselectivity of the membranes, shedding light on the behavior of both membranes across a range of salt concentrations and in the presence of real brine solutions.

The performance of a lab-scale RED unit was evaluated in a real environment by testing two real brine discharges for distinct origins and salinities, but both coming from saltworks: Margi saltworks brine and Nubia saltworks brine were used as feed solutions.

https://doi.org/10.1021/acsomega.4c08651
ACS Omega 2025, 10, 29980−29991

2. EXPERIMENTAL PART

2.1. Materials. Two different homogeneous ion exchange membranes (IEMs), developed by Fujifilm Manufacturing Europe BV (The Netherlands) and Suez (France), were investigated: Fujifilm AEM Type 10- and Fujifilm CEM Type 10-incorporated reinforced polyolefin and Suez AEM (AR103) and CEM (CR67U) are reinforced with ultrathin nonwoven cloth. Full details on the properties of these IEMs can be found in Table 1.

Table 1. Membrane Properties According to the Supplier's Specifications

	Fujifilm[30]		Suez[31]	
membrane	AEM Type 10	CEM Type 10	AEM-AR103U	CEM-CR67U
thickness dry (μm)	125	135	130	150
electrical resistance (Ω cm^2)	1.7	2.0	1.4	2.0
permselectivity	95	99	90	90
IEC (m_{eq} g^{-1})	1.8	1.5	2.37	1.92
water permeation (mL bar^{-1} m^{-2} h^{-1})	6.5	6.5		

The information in Table 1 has been collected from the data sheets of membrane manufacturers when available.

Fujifilm membranes were supplied in the dry form before the use and were activated in 0.5 M NaCl, while Suez membranes were received in wet form (deionized water) and were immersed in 0.5 M NaCl for activation. All of the experiments were repeated twice with a maximum discrepancy of less than 5%; average values were reported in the manuscript.

2.2. Ion Sorption. Following water presoaking, these membranes were then immersed in 30 mL of an artificial aqueous solution of 0.5, 1, and 5 M NaCl and real Margi brine for 48 h to reach equilibrium, after which the membranes were transferred to water of a known volume of 30 mL for a further 48 h. During the second soaking period, the absorbed co-ions (in the form of relevant salts) were released into the water. The concentration of co-ions in these water samples was later measured by ion chromatography. A uniform concentration during the soaking process was guaranteed by keeping the system under mechanical agitation: in particular, a magnetic stirrer and a rotational speed of 1500 RPM were used to this aim. All sorption tests were carried out at room temperature (i.e., ~25 °C).

The cation exchange membranes were moved into a 0.5 M HNO_3 solution, and anion exchange membranes were transferred into a 0.5 M NaOH solution of a known volume (30 mL) for a further 48 h to release the adsorbed counterions. The solution was changed after each 48 h to make sure that all counterions were released. During this soaking period, the adsorbed ions were released into HNO_3 and NaOH. The concentration of counterions in HNO_3 and NaOH was later measured by ion chromatography.

The concentration of ions in CEMs and AEMs was measured by ion chromatography. A single desorption procedure was sufficient to extract all co-ions from the membranes; as a matter of fact, a negligible co-ion concentration was found in the second desorption solution.

The co-ion and counterion concentrations in the membrane were calculated as follows

$$C^{m}_{\text{co-ion}_i}\left[\frac{\text{mol}}{\text{kg}_{\text{water}}}\right] = \frac{10^{-3} \times m_i^{\text{sol}}\,[\text{ppm}] \times M_{\text{sol}}\,[\text{g}]}{\text{MW}_i \times W_{\text{u}} \times M_{\text{dry}}\,[\text{g}]} \quad (1)$$

$$C^{m}_{\text{counter-ion}_i}\left[\frac{\text{mol}}{\text{kg}_{\text{water}}}\right] = \frac{10^{-3} \times m_i^{\text{sol}}\,[\text{ppm}] \times M_{\text{sol}}\,[\text{g}]}{\text{MW}_i \times W_{\text{u}} \times M_{\text{dry}}\,[\text{g}]} \quad (2)$$

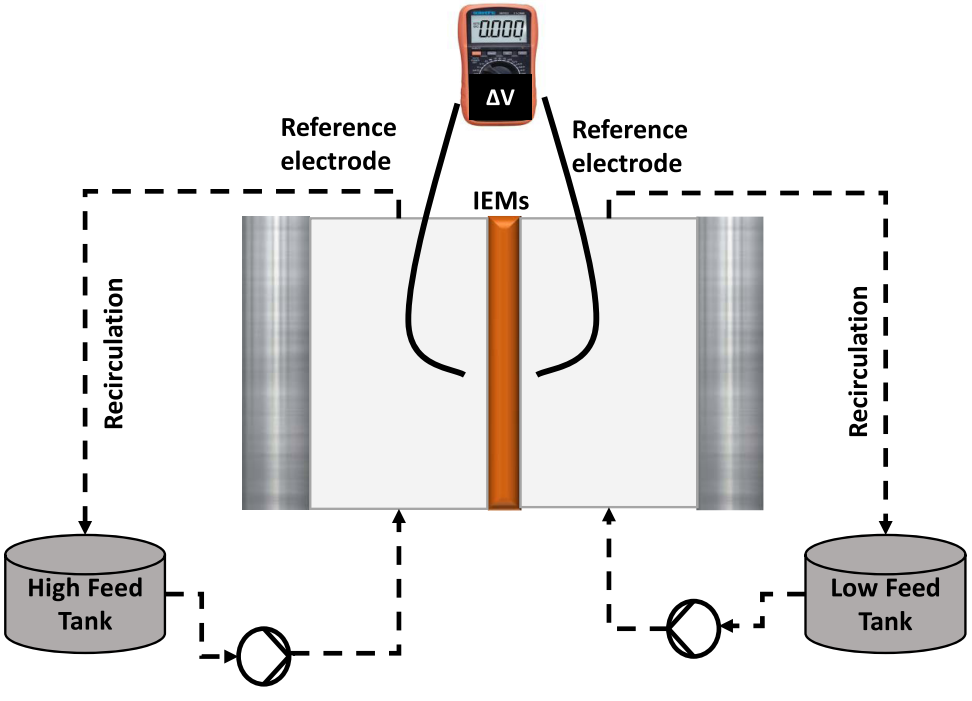

Figure 2. Characterizing permselectivity in a two-compartment system.

https://doi.org/10.1021/acsomega.4c08651
ACS Omega 2025, 10, 29980−29991

where $C^{m}_{co/counter\text{-}ion_i}$ is the mole of ions per kg of membranes (i.e., water and ions in the volume of the swollen membrane), m_i^{sol} is part per million of ions (ppm), M_{sol} is the mass of desorption solution, and MW_i is the molar weight of the ion, W_u is water uptake, and M_{dry} is the dry mass of the membrane in grams.

The corresponding fixed charge group concentration in each IEM was determined as the difference between the concentration of counterions and the concentration of co-ions.

2.3. Permselectivity. A two-compartment cell was operated at a temperature of 30 °C to determine the membrane potential, as shown in Figure 2. This temperature is representative of the temperature of real discharged bitterns. The membranes were conditioned in a 0.5 M NaCl solution overnight before measurements were taken. After that, the membrane was placed between the compartments where two solutions at different concentrations were fed, and the membrane potential was measured. During the permselectivity test, the real Margi brine and a synthetic solution of 5 M NaCl were used for both IEMs. More precisely, we conducted tests on CEMs and AEMs across two hypersaline concentration gradients, specifically in (I) 0.06 M/5 M and (II) 0.06 M/Margi real brine solution pairs.

To reduce polarization phenomena, the real Margi brine and synthetic solutions were continuously recirculated through the compartments using two gear pumps, operating at a flow rate of 2 cm s^{-1} and maintained at a temperature at 30 °C. Finally, the permselectivity (α) was calculated by taking the ratio between the measured membrane potential (V) and the theoretical membrane potential (V), as outlined in eq 3.

$$\alpha\,[-] = \frac{\Delta V_{measured}}{\Delta V_{theoretical}} \tag{3}$$

Here, $\Delta V_{theoretical}$ is measured by the Nernst equation, which is reported in eq 4 for the case of saline solutions composed of NaCl only.

$$\Delta V_{theoretical}\,[V] = \frac{RT}{zF}\ln\left(\frac{a_c}{a_d}\right) \tag{4}$$

Here, R is the universal gas constant (J mol^{-1} K^{-1}), T is the absolute temperature (K), F is the Faraday constant (C mol^{-1}), a_c and a_d are the activities of the concentrated and diluted solutions (mol L^{-1}), respectively, and z is the ion valence (−). The Pitzer model was used to determine the activity coefficient.[32]

For real brine solution, $OCV_{theoretical}$ was calculated by the following equation.

$$\Delta V_{theoretical}\,[V] = \frac{RT}{F}\ln\prod_i \frac{(\gamma_{\pm}^{c}C^{c})^{1/z_i}}{(\gamma_{\pm}^{d}C^{d})^{1/z_i}} \tag{5}$$

Here, $\gamma_{\pm}^{c}$ and $\gamma_{\pm}^{d}$ represent the activity coefficient of the ion, while C^c and C^d represent the high- and low-concentration solutions, respectively.

2.4. Reverse Electrodialysis Stack. A conventional lab-scale RED stack (REDstack B.V., Netherlands) comprising five piled cell pairs (see Figure 1) with an active membrane area of 10 × 10 cm^2, as described in our previous paper,[33] was investigated. The IEMs were separated by placing a polyamide woven spacer that was 270 μm thick (Deukum, Frickenhausen, Germany) to create feed channels. At the endplates, a pair of 10 × 10 cm^2 two Ru−Ir oxide-coated titanium electrodes (Magneto Special Anodes BV) were used as the cathode and anode. Before each RED test, a pretreatment process was used to condition the membranes by keeping the stack in the solutions to be tested overnight.

RED experiments were carried out at different flow velocities (1−3 cm/s), as detailed in Table 2. High H_c and low L_C feed solutions were fed to the stack at the same temperature of 30 °C. This value was chosen because it can be considered representative of the temperature at which the bittern is disposed of during the summer season. Clearly, taking the bittern during a different season means taking a solution with a different concentration and temperature. The latter is expected to provide worse results during the colder season, as can be easily inferred from eq 5. 0.1 M $K_3Fe(CN)_6/K_4Fe(CN)_6$ and 0.6 M NaCl are used as an electrolyte rinse solution. The feed solutions were fed to the stack by Masterflex L/S peristaltic pumps (BT601S from Lead Fluid Technology, Co., Ltd., China). A custom-made heating bath was employed to keep the feed solutions at the desired temperature. The solutions' conductivity was monitored by a conductivity meter (3320, Xylem). Two pressure transducers (the one for the concentrated stream, the other for the diluted one) were installed at the inlet of each stream to monitor the pressure drops in the unit. To quantify measurement uncertainty, all experiments were repeated three times, and experimental results were averaged.

Table 2. Scenario Configurations for the Experimental Campaign[a]

scenario	flow velocity (cm/s)	temperature (°C)
Margi-A	1 to 3	30
Margi-B		
Nubia-A		
Nubia-B		
Margi-S		
synthetic solution	1	

[a]"A" means untreated brine, "B" means treated brine, and "S" is spiked brine.

As feeds, two different saltworks bitterns were investigated (i.e., Margi and Nubia). In addition, in accordance with the SEArcularMINE project idea, these brines might be either directly sent to a RED unit for electricity production or pretreated by removing Mg^{2+} ions in an upstream crystallizer and reducing the brine salinity. The former case is hereafter regarded as untreated brine, case A; the latter is hereafter regarded as treated brine, case B. Relevant compositions are reported in Section 2.6. Depending on the concentration of the alkaline solution (i.e., NaOH) employed in the crystallizer for the reactive precipitation of $Mg(OH)_2$, the resulting Mg-free brine can exhibit a different Na^+ concentration. According to some promising operating conditions adopted in the framework of the SEArcularMINE project and not discussed here for the sake of brevity, a third type of Margi brine was also investigated. This brine was named Margi-S spiked brine (Margi-S); it exhibits a negligible amount of Mg^{2+} and a Na^+ concentration higher than that of Margi-B. Its composition is also reported in Section 2.6.

2.5. Polarization Curve and Power Measurement. The measurements were done by connecting two multimeters (Fllike-175) one in series and one in parallel to the RED stack (the range varying from 0 to 10 A). They were used to

https://doi.org/10.1021/acsomega.4c08651
ACS Omega 2025, 10, 29980−29991

Table 3. Composition of Real and Treated Brines of Saltworks

	composition (g/L)							
type of brine	Na^+	K^+	Mg^{2+}	Ca^{2+}	Cl^-	Br^-	SO_4^{2-}	TDS (g/L)
Margi-A	56.10	13.27	49.40	0.05	181.69	2.48	61.59	364.60
Margi-B	27.48	1.87	0.006	0.003	24.20	0.002	8.073	62.28
Nubia-A	72.59	11.02	38.65	0.002	186.29	2.18	48.55	359.28
Nubia-B	28.40	1.59	0.01	0.004	26.65	0.31	7.30	64.26
Margi-S	96.07	0.69	0.01	0.003	102.46	0.05	26.07	225.35

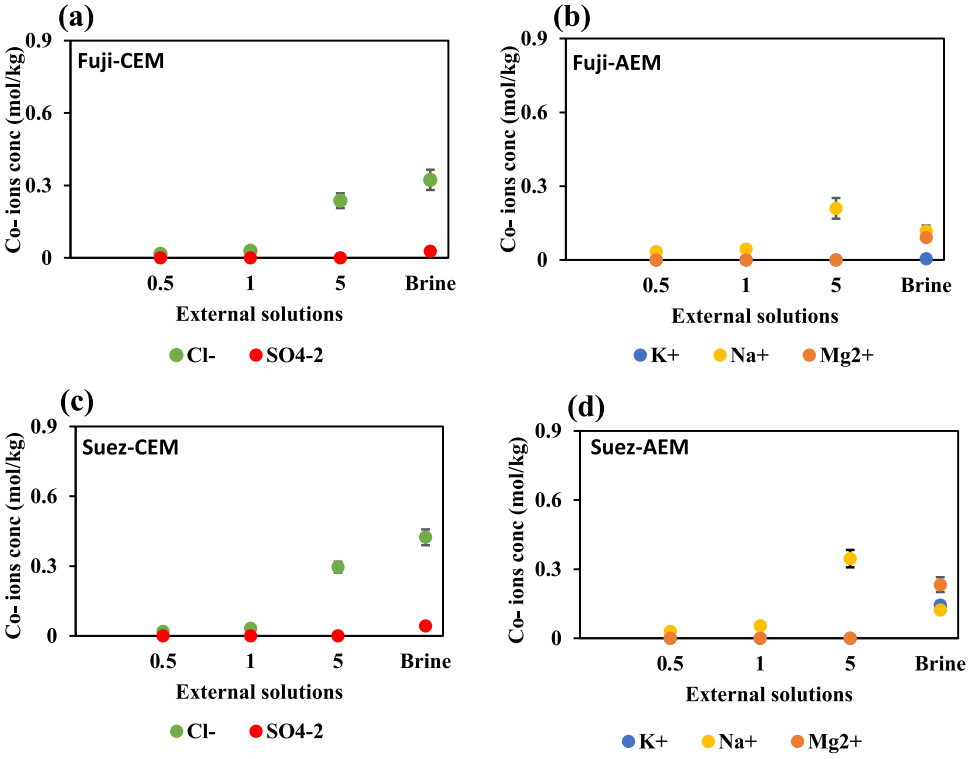

Figure 3. Concentration of co-ions (expressed in mol/kg) in Fujifilm and Suez IEMs as a function of saline solutions. Margi is employed as waste brine. 0.5, 1, and 5 M refer to artificial solutions composed of NaCl only. (a) Fujifilm CEM; (b) Fujifilm AEM; (c) SUEZ CEM; (d) SUEZ AEM.

measure the polarization curve, i.e., the current−voltage ($I-V$) curve and the corresponding power P produced. In order to do so, a variable load resistance R_{load} (BK Precision, 8540) was employed. Power generation per unit cell pair area is defined as power density (W/m^2).

$$P_d\left[\frac{W}{m_{cp}^2}\right] = \frac{P}{NA} \tag{6}$$

Here, N is the number of cell pairs (5) and A (0.01 m^2) is the active area of membranes.

The blank resistance R_{blank} (electrode compartment resistance) has a significant effect on the power density when a small-scale RED unit composed of a few cell pairs is adopted. However, using a large number of cell pairs (e.g., in a full-scale stack) where the contribution given by electrode compartments to total stack resistance (R_{stack}) becomes negligible on the power density. R_{blank} was measured by mounting the RED unit with only one end membrane, and electrode compartments were fed with the electrode rinse solution (ERS) only. Once measured, the corrected power density ($P_{d,corr}$) can be computed by subtracting R_{blank} from stack resistance R_{stack} according to eq 7. The resistance used to calculate the power density is relevant to the cell pairs only, and it is named R_{cells} ($R_{cells} = R_{stack} - R_{blank}$). R_{stack} is inferred from the slope of the measured $I-V$ curves.[22]

$$P_{d,corr}\left[\frac{W}{m_{cp}^2}\right] = \frac{OCV^2}{NAR_{load}\left(1 + \left(\frac{R_{cells}}{R_{load}}\right)\right)^2} \tag{7}$$

Here, OCV is the open circuit voltage. Pressure drop measurements were used to calculate the pumping power density. As a result, net power density is calculated as the difference between the gross power density (e.g., eq 7) and the pumping power density.

2.6. Ion Chromatography. Ion chromatography (Metrohm, Italy) analysis was employed to quantify the ions present in Trapani real and treated brine at the inlet of the RED unit operated under the experimental conditions shown in Table 2. The samples for the analyses were collected in summer when the waste brine (i.e., bittern) was typically disposed of. These were analyzed at room temperature at which ion chromatography was calibrated. 3.2 mM Na_2CO_3 + 1 mM $NaHCO_3$ was used as an eluent for the anion column (882 compact IC flex), whereas 5.5 mM phosphoric acid solution was used as an eluent for the cation column (930 compact IC flex). The

https://doi.org/10.1021/acsomega.4c08651
ACS Omega 2025, 10, 29980−29991

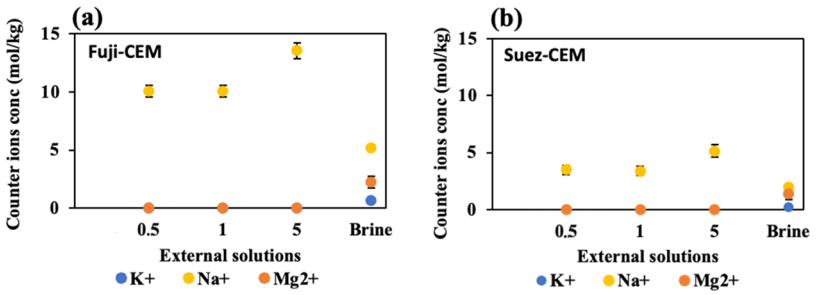

Figure 4. Counterion concentration in CEMs as a function of saline solution: (a) Fujifilm CEM and (b) Suez CEM. Margi is employed as waste brine; 0.5, 1, and 5 M refer to artificial solutions composed of NaCl only.

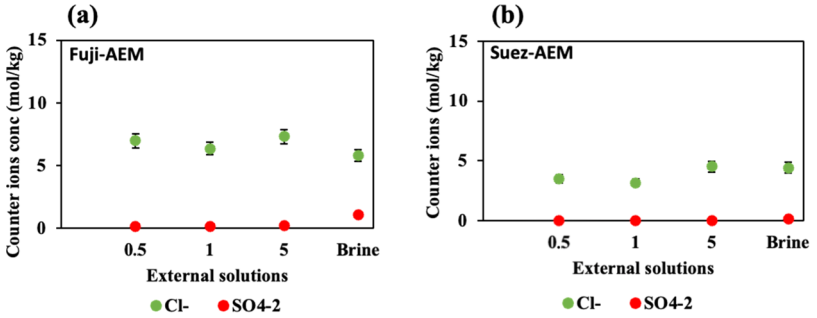

Figure 5. Counterion concentration in AEMs as a function of saline solution: (a) Fujifilm AEM and (b) Suez AEM. Margi is employed as waste brine. 0.5, 1, and 5 M refer to artificial solutions composed of NaCl only.

measured compositions are reported in Table 3; relevant ion chromatography analyses were repeated twice, and a maximum discrepancy of always lower than 4% was found.

3. RESULTS AND DISCUSSION

3.1. Co-Ion Concentration in IEMs. The concentrations of both counterions and co-ions within the ion exchange membranes (IEMs) were quantified. To satisfy the electroneutrality of the membrane (and of the solution), the uptake of 1 equiv of counterions cannot occur without exchange with another equivalent of co-ions or in the form of a neutral salt. Predominantly, the counterions found within the membrane are closely linked to the fixed charges residing within the polymer matrix. However, a minute fraction of counterions was detected because of the nonideal permselectivity of the membranes.

The presence of co-ions is effectively blocked from permeating the membrane, primarily because they face repulsion from the fixed charge groups. These charge groups create an electric potential, referred to as the Donnan potential, at the interface between the membrane and the surrounding solution, as described initially by Donnan in 1924.[34] As the concentration of the external salt increases, this electric potential diminishes due to the screening effect of charged species, thereby enabling a greater intake of co-ions. Moreover, by increasing the concentration of the external solution, the higher difference in ions' activity between the solution phase and the membrane phase favors co-ion uptake in the membrane. Thus, as expected, the concentration of co-ions (i.e., Cl^-) in Fujifilm CEM and Suez CEM and (i.e., Na^+) in both AEMs increases with increasing artificial salt solution concentration, as shown in Figure 3.

The Donnan potential exhibits an inverse relationship with the valence of counterions.[35] Consequently, the introduction of divalent counterions, such as magnesium in anion exchange membranes (AEMs) and sulfate in cation exchange membranes (CEMs), serves to diminish the Donnan potential. This reduction, in turn, contributes to an augmented co-ion concentration within the membrane. The co-ions Na^+ and Mg^{2+} in Suez AEM were higher than those pertaining to Fujifilm AEM. Conversely, similar co-ion concentrations were found in the two CEMs.

3.2. Counterions in CEMs. Counterions in the cation exchange membranes (swollen membranes) are reported in moles per kilogram in Figure 4. At 0.5 and 1 M, the measured counterion concentration was similar and low compared to 5 M solution because at high solution concentrations, all fixed charge groups are occupied due to the higher difference in activity of the ions in solution with respect to the membrane phase. Moreover, more counterions are sorbed in Fujifilm CEM than in Suez CEM, despite the lower IEC (Table 1) with respect to Suez CEM, thus indicating the higher performance of Fujifilm CEM. When a bittern is adopted as a saline solution, the concentration of Mg^{2+} in Fujifilm CEM is 2.27 mol/kg, which is half of that of sodium due to its double charge (Figure 4a). The Suez CEM exhibits a magnesium ion concentration of 1.42 mol/kg, while the sodium ion concentration is 1.96 mol/kg (only ∼ 27% less, Figure 4b). The latter is likely due to the strong interactions between Mg^{2+} ions (having a larger hydrated radius) and the fixed charge group of Suez CEM. Both IEMs show a reduction in the total counterion concentration for the case of the real brine, and this might be a consequence of the screening effect of accumulating ions in the solution, thus leading to a decrease in the strength of electrostatic forces and a reduction of the Donnan exclusion effect. Moreover, it is important to consider that sulfonic groups (i.e., the ion exchange groups present in the CEMs) have a higher affinity for Mg^{2+} than for Na^+,[36] but one Mg^{2+} ion interacts with two sulfonic groups, while the Na^+ interacts in ratio 1:1 with membrane ion exchange groups.

https://doi.org/10.1021/acsomega.4c08651
ACS Omega 2025, 10, 29980−29991

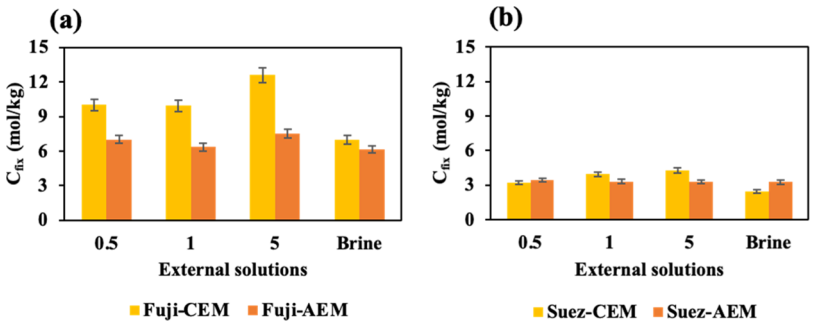

Figure 6. Fixed charge group concentrations for Fuji and Suez IEMs as a function of saline solution. The fixed charge group concentration was measured as the difference between the co-ion and counterion concentrations in membranes. Margi is employed as waste brine. (a) Fujifilm IEMs; (b) SUEZ IEMs.

3.3. Counterions in AEMs. Similar tests were performed to obtain the concentration of counterions in the Fujifilm and Suez anion exchange membranes. The counterion concentration of Cl^- in both AEM Fujifilm and Suez somehow slightly increases when the artificial aqueous solution of NaCl only increases from 0.5 to 5 M, expressed in mol/kg swollen membranes (Figure 5a,b). It is also evident that the monovalent Cl^- is preferably absorbed when the membranes are equilibrated in a brine solution, as expected. The counterion Cl^- in Fuji AEM appeared to be greater than that observed in Suez AEM, thus suggesting a better performance of Fujifilm AEM compared to Suez ones.

3.4. Fixed Charge Group Concentration in Membranes. The fixed charge group concentration in each IEM was determined as the difference between the corresponding counterion concentration minus the co-ion concentrations, and it is shown as a function of artificial and real brine solution in Figure 6. In other words, data reported in Figure 6 can be easily inferred from the corresponding data reported in Figures 3,4, and 5.

Figure 6 shows that the fixed charge concentration is larger for the Fujifilm membrane compared to the Suez one; this is expected to allow them to be more efficient in driving counterion fluxes. The fixed charge concentration is found to be dependent on the solution salinity and type employed, although IEMs are of the same type, and the number of fixed charges is expected to be the same. Clearly, the dependence of the fixed charge group concentration on salinity shown in Figure 6 is not surprising because the water uptake is dependent on salinity as well.

3.5. Permselectivity. Membrane permselectivity is a crucial indicator of its ability to selectively transport counterions over co-ions. It is noteworthy that the majority of commercially available ion exchange membranes exhibit permselectivity exceeding 0.90. However, prior research has demonstrated that the permselectivity of these membranes is notably influenced by the concentration and composition of the test solutions. While the permselectivity can approach the ideal value of 1.00 in diluted solutions, it tends to decrease in more concentrated solutions or brines.[37] Consequently, we conducted tests of CEMs and AEMs across two hypersaline concentration gradients, specifically in (I) 0.06 M/5 M and (II) 0.06 M/Margi real brine solution pairs.

Figure 7 provides a comparative analysis of permselectivity data for Fujifilm and Suez IEMs, illustrating their responses to NaCl and brine solution concentration gradients while maintaining a constant temperature of 30 °C. In solution

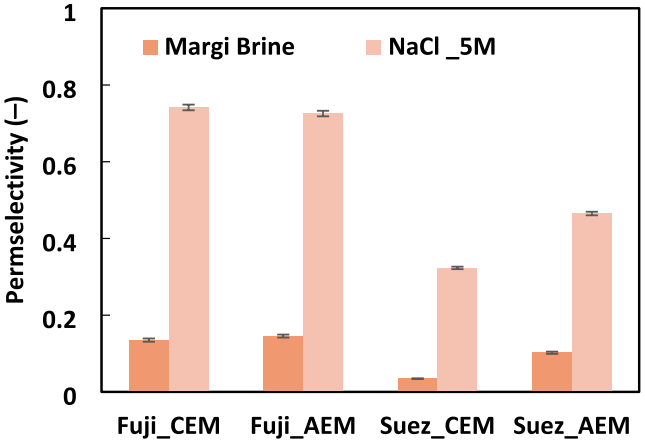

Figure 7. Permselectivity of Fujifilm and Suez IEMs at 5 M NaCl and real Margi-A brine solution (temperature: 30 °C and flow velocity: 2 cm/s).

(0.06/5 M NaCl), the measured permselectivity for the Fujifilm CEM and AEM was much higher than that pertaining to Suez IEMs. The high charge density of Fujifilm CEM and AEM leads to a good co-ion repulsion and permeates the counterions, while the lower charge density of Suez CEM and AEM causes a larger co-ion transport from the high- to low-concentration compartment.

Furthermore, in the real brine solution, the values were significantly reduced for all of the IEMs; even a value lower than 0.1 was measured for Suez CEM. The presence of bivalent ions, as those present in Margi brine, reduces the permselectivity of IEMs because of the shielding effect of bivalent ions on the fixed charge groups (reduction of the Donnan potential), which reduces the ability of the membrane to exclude co-ions in the membrane. The very low permselectivity values of Suez IEMs can be ascribed to its porous structure, which leads to inefficient Donnan exclusion, possibly due to the presence of defects or the occurrence of interstitial concentration polarization.

It is worth noting that average permselectivity $\left(\frac{\alpha_{AEM} + \alpha_{CEM}}{2}\right)$ can also be inferred from the ratio of the OCV values measured for the whole RED stack and reported in Figure 9 and theoretical OCV values, which can be calculated via eq 5.[38] Resulting average permselectivities were found to be very similar to those reported in Figure 7, thus confirming the soundness of the permselectivity measurement procedure.

https://doi.org/10.1021/acsomega.4c08651
ACS Omega 2025, 10, 29980−29991

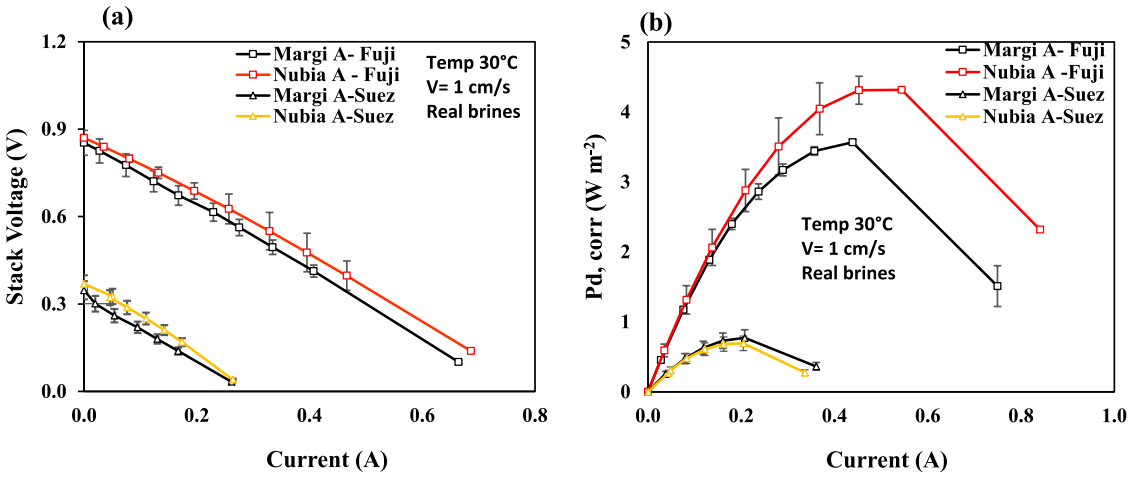

Figure 8. RED unit (assembled with two different membranes) performance at 30 °C for the case of the two different bitterns: (a) stack voltage versus current and (b) corrected power density versus current. Flow velocity: 1 cm/s.

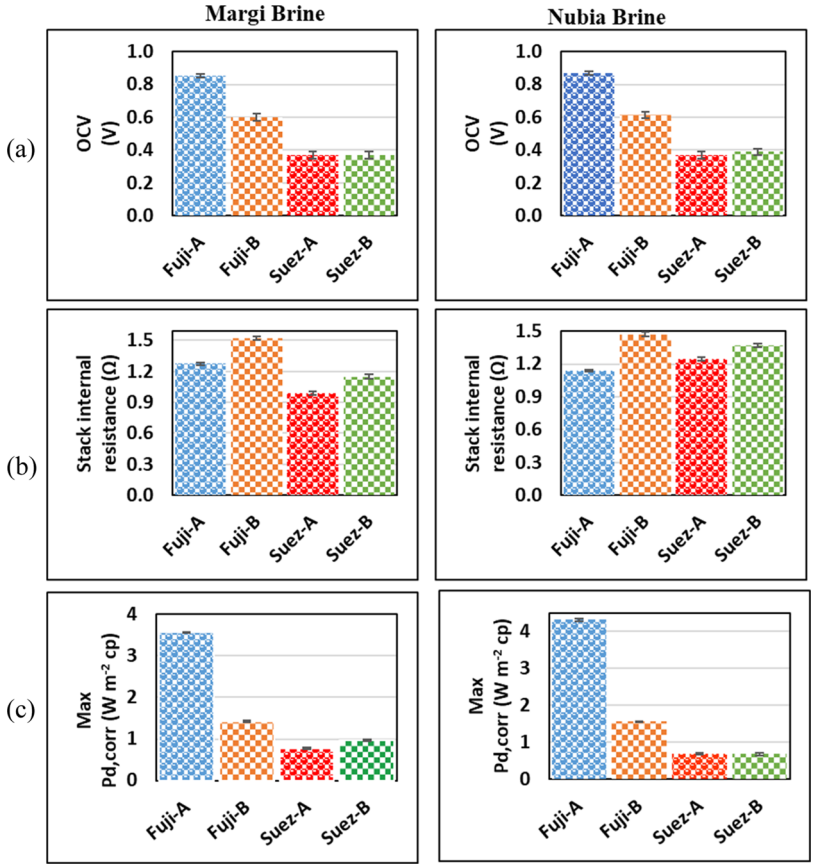

Figure 9. Experimental (a) OCV, (b) R_{stack}, and (c) Max $P_{d,corr}$ as functions of IEMs and feed bittern. Five cell pair stack fed with Margi brine (left) and Nubia brine (right), velocity = 1 cm s^{-1}, and T = 30 °C.

3.6. RED Study Performance with Real Bitterns. This section is devoted to the experiments carried out with the laboratory-scale RED unit. The higher compartment of the RED stack was fed by natural brine discharged from two distinct origin (Margi and Nubia) brines under investigation containing 364.60 and 359.28 g/L total dissolved solids (TDS), respectively. The lower compartment was fed by synthetic solutions (i.e., NaCl only) of 0.06 M equivalent to natural freshwater.

Figure 8 illustrates current (A) versus stack voltage (V) and current versus power density curves for the RED unit assembled with the two different IEMs (Fujifilm and Suez) for both brine and artificial solutions at a constant temperature of 30 °C and at 1 cm/s flow velocity.

The maximum corrected power density was obtained by a RED stack equipped with Fujifilm membranes and fed with Nubia real brine: $P_{d,corr}$ reached a maximum of 4.32 W/m^2 at a current of 0.40 A (OCV was 0.87 V and stack resistance R_{stack} was 1.14 Ω). On the other hand, the poorest performance was

https://doi.org/10.1021/acsomega.4c08651
ACS Omega 2025, 10, 29980−29991

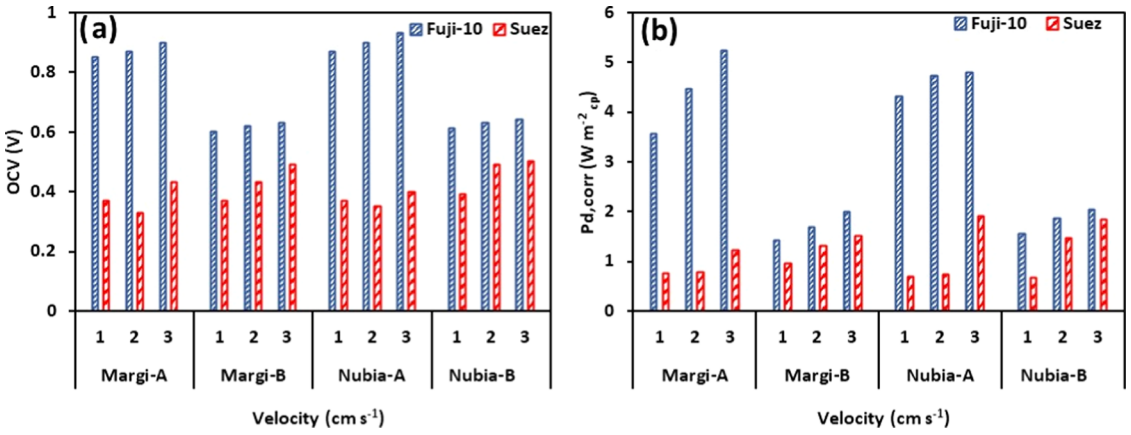

Figure 10. Effect of flow velocity on the RED stack performance: (a) open circuit voltage and (b) corrected power density.

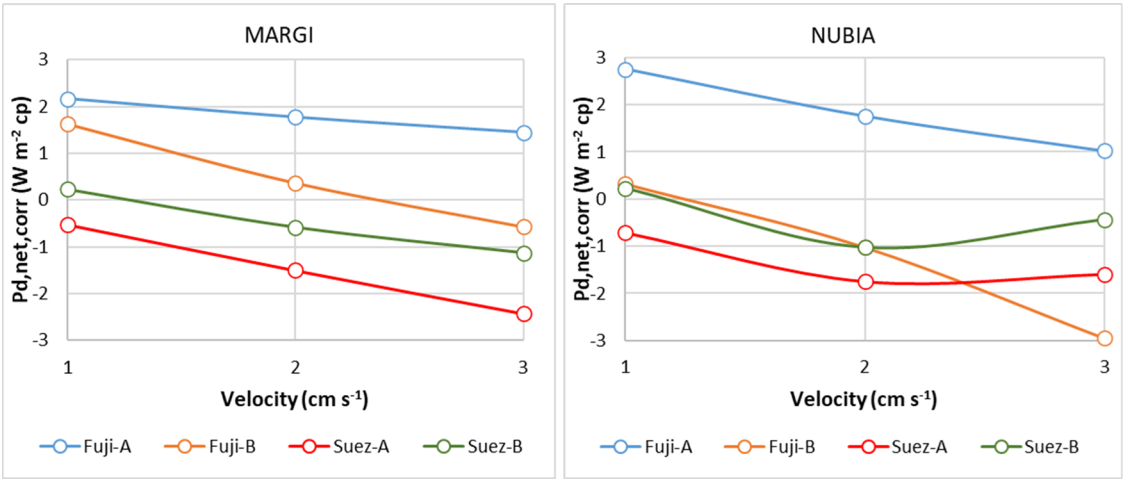

Figure 11. Effect of flow velocity on the corrected net power density produced by the RED stack.

detected by the stack fed with real Nubia brine and Suez IEMs: maximum $P_{d,corr}$ and current fell down to 0.69 W/m^2 and 0.17 A, respectively. This difference is due to the much lower OCV (due to the much lower permselectivity) because R_{stack} was found to be similar in the two cases (R_{stack} = 1.25 Ω). As expected from the basis of the data collected on the two membranes (see Sections 3.1 to 3.6), the stack equipped with Fujifilm IEMs performs much better than that provided with Suez membranes.[37] Margi-A and Nubia-A real brines are quite similar in terms of overall salinity and conductivity. The main difference is that Nubia has a higher amount of Na^+ and a lower amount of divalent ions. This difference does not seem to have a clear effect on the stack equipped with Suez membranes. Conversely, this is not the case for the Fujifilm stack where the higher amount of divalent ions leads to a significant performance reduction, fully in accordance with literature findings.[9] Overall, the values of power density reported in Figure 8 for the real brines are comparable with those reported in the literature for the same solutions,[9−22] while other comparisons with other published works are not possible due to the very different composition.

A comparison with the other bitterns available along the SEArcularMINE chain is reported in Figure 9 in terms of OCV, stack resistance, and maximum corrected power density.

Comparing results relevant to original (i.e., A) and treated (i.e., B) brines, Figure 9 shows that the OCV reduces when the stack is fed with type-B brines for the case of Fujifilm IEMs. Conversely, only slight differences are observable when the stack is equipped with Suez IEMs. Thus, although type-A brines have a higher amount of divalent ions, this is more than counterbalanced by the larger salinity for Fujifilm IEMs. On the contrary, these two effects are comparable in the case of the stack with Suez IEMs. Similarly, a larger stack resistance is exhibited by the stack equipped with Fujifilm IEMs and fed by type-B brines, while comparable resistance was found for the Suez stack. As a result of a larger OCV and lower electrical resistance, the Fujifilm stack fed by type-A brines performs much better in terms of power density than the stack operated with type-B brines. As a result of similar OCV and ohmic stack resistance, Suez stack performance is slightly dependent on the real brine type used.

These results confirm that membranes are critical components of the RED stack that limit the SGP recovery performance. The electrical membrane resistance, permselectivity, ionic resistance, membrane swelling degree (SD), and ion exchange capacity (IEC) are all critical properties of ion exchange membranes. Prior studies highlighted the importance of commercially available IEMs designed specifically for RED applications with superior physical and electrochemical features that boost energy efficiency and promote the wider implementation of the technology.[39]

3.7. Effect of the Flow Rate on RED Stack Performance. The flow velocity of streams in the RED channels can alter the rate of ion migration through ion exchange

https://doi.org/10.1021/acsomega.4c08651
ACS Omega 2025, 10, 29980−29991

membranes, hence affecting the performance of the RED stack. Figure 10 shows the effect of the flow velocity on the OCV (Figure 10a) and maximum $P_{d,corr}$ (Figure 10b) for the different investigated brines (dilute concentration equal to 0.06 M, T = 30 °C).

As expected, the higher the velocity in the channels, the higher the OCV and the power density. Typically, changing the velocity in a RED unit affects three different phenomena: (i) the streamwise variation of the salinity gradient, also named axial concentration polarization, and relevant ohmic variations, (ii) the cross-stream concentration polarization, and (iii) the pressure drops.[40,41] (iii) Pumping power requirements are not investigated in the present work. (ii) A velocity of 1 cm/s along with the adoption of very concentrated brines is known to be sufficient to avoid any cross-stream concentration polarization effects by providing polarization factors very close to 1.[42] Thus, increasing the velocity from 1 to 3 cm/s is not expected to produce any beneficial/detrimental effects of this phenomenon. (i) This is not the case for the axial concentration polarization; higher velocity means lower residence times and lower salinity gradient drops: the higher the velocity of the streams, the lower the driving force reduction along the stack. Similarly, during the OCV tests, higher velocities counteract the salinity gradient reduction due to diffusive and osmotic phenomena. Thus, in all cases, a higher velocity leads to better performance. Pressure losses should also be taken into account in order to monitor the net variables.[40,41]

In order to do so, we used the pressure drops measured to calculate the pumping power density. The net power density reported in Figure 11 is obtained by subtracting it from the gross power density. As can be seen in the figure, although increasing the feed solution velocity can be beneficial for gross variables, the pumping power can easily exceed the gross power produced, thus resulting in net power densities being negative. More precisely, only when the velocity is equal to 1 cm/s is a positive power generated by the RED unit. Furthermore, this value is of interest only when Fujifilm IEMs are adopted. Clearly, it should be mentioned that the stack investigated is not specifically tailored to minimize pressure losses, and actions could be implemented to increase the net power density. As a consequence, most of the cases investigated will not be suitable for future electric power generation.

3.8. Performance of RED Units Fed with Spiked Brine.

In this section, the RED stack equipped with Fujifilm/Suez membranes was investigated using spike brine. The tests were conducted at 1, 2, and 3 cm s^{-1}.[27] Variations of the power density and the OCV are shown in Table 4. As can be seen, again, the performances of the stack equipped with the Fujifilm membranes are better compared to the Suez stack: ohmic resistances are more similar than before, but the clear difference in OCV leads to a significant difference in terms of power output. Increasing the feed flow rate results in beneficial performance enhancement for the same reasons discussed in the previous section.

Table 4. Performance of the RED Unit Fed by the Spike Brine as a Concentrate and 0.06 NaCl Solution as a Dilutent

spike brine						
	Fujifilm Type 10			Suez		
velocity, cm/s	$P_{d,corr}$, W/m^2	OCV, V	R_{stack}, Ω	$P_{d,corr}$, W/m^2	OCV, V	R_{stack}, Ω
1	2.97	0.80	1.34	1.55	0.55	1.25
2	3.34	0.85	1.36	2.36	0.61	1.05
3	4.29	0.87	1.14	4.00	0.64	0.78

Results relevant to the spiked brine can be compared to those relevant to a different feed. Unfortunately, a direct comparison is not possible due to the nature of the brines tested. With this respect, the aim of the work is not that of testing RED units performance by letting the feed composition vary to better understand the effect of each ion. Rather, the idea is that of testing RED units with different brines which might be available within the SEArcularMINE chain, e.g., depending on the operating conditions of upstream units as the magnesium crystallizer.

To this aim, the corrected power outputs (i.e., $P_{d,corr}$) of RED units fed with Margi-A and -B brines are compared with those relevant to Margi-S (Table 4, velocity = 1 cm/s case). Fujifilm stacks provided the best results when operated with Margi-A (~3.5 W/m^2) followed by Margi-S (~3 W/m^2) and Margi-B (~1.5 W/m^2), thus suggesting that the overall concentration of the brine is the prominent factor in the performance. Conversely, the SUEZ stack performed better when operated with the spiked brine Margi-S (~1.5 W/m^2), although the differences were quite small.

However, it should be kept in mind that there is room to improve the performance of stacks operated with multi-ion solutions; as a matter of fact, the best performance can be obtained when NaCl-only aqueous solutions are employed. A stack operated with 5 M artificial brine would lead to $P_{d,corr}$ values of about 6 and 3 W/m^2 for Fujifilm and Suez IEMs, respectively.[33]

4. CONCLUSIONS

This study quantifies the performance of ion exchange membranes from two manufacturers concerning parameters such as fixed charge density and permselectivity. The electrochemical performance of these ion exchange membranes was assessed within a RED system, measuring power generation, stack resistance, and open cell potential.

In the present work, we investigate the behavior of various types of solutions, including artificial brines at different concentrations and different real brines available within the SEArcularMINE process chain. When exposed to artificial NaCl and real brine solutions, we report the equilibrium ion concentrations in commercially available Fujifilm Type 10 and Suez ion exchange membranes. This evaluation allows us to assess co-ion, counterion, and fixed charge concentrations within the membranes. Membrane permselectivity was also assessed.

Laboratory-scale RED units equipped with the two different IEMs were tested, and they were also operated with different feed brine streams. In particular, when the RED unit is equipped with a Fujifilm IEM and fed by high-salinity streams, the power generated might be compatible with future power generation systems.

By comparing the two commercial IEMs tested, collected results, both on membrane features and on stack performance, suggest that the Fujifilm membranes are more suitable for RED applications than SUEZ ones, although the former are more sensitive to bivalent ion presence. Thus, future efforts on membrane manufacturing for RED should be devoted to combining the strength points of the two IEMs.

https://doi.org/10.1021/acsomega.4c08651
ACS Omega 2025, 10, 29980−29991

AUTHOR INFORMATION

Corresponding Author

Alessandro Tamburini − *Dipartimento di Ingegneria, Università degli studi di Palermo, 90129 Palermo, Italy; ResourSEAs SRL, 90128 Palermo, Italy;* orcid.org/0000-0002-0183-5873; Email: alessandro.tamburini@unipa.it

Authors

Syed Abdullah Shah − *Dipartimento di Ingegneria, Università degli studi di Palermo, 90129 Palermo, Italy; Consiglio Nazionale delle Ricerche (CNR), Istituto per la Tecnologia delle Membrane (ITM), 8036 Rende, CS, Italy*

Enrica Fontananova − *Consiglio Nazionale delle Ricerche (CNR), Istituto per la Tecnologia delle Membrane (ITM), 8036 Rende, CS, Italy;* orcid.org/0000-0002-2506-0160

Andrea Cipollina − *Dipartimento di Ingegneria, Università degli studi di Palermo, 90129 Palermo, Italy;* orcid.org/0000-0003-0570-195X

Alberto Figoli − *Consiglio Nazionale delle Ricerche (CNR), Istituto per la Tecnologia delle Membrane (ITM), 8036 Rende, CS, Italy;* orcid.org/0000-0002-3347-0506

Giorgio Micale − *Dipartimento di Ingegneria, Università degli studi di Palermo, 90129 Palermo, Italy*

Complete contact information is available at: https://pubs.acs.org/10.1021/acsomega.4c08651

Author Contributions

S.A.S.: investigation, methodology, validation, formal analysis, investigation, writing—original draft, and visualization. E.F.: methodology, conceptualization, validation, resources, and supervision. A.C.: conceptualization, validation, resources, supervision, project administration, funding acquisition, and writing—review and editing. A.T.: methodology, resources, supervision, and writing—review and editing. A.F.: resources, supervision, project administration, and funding acquisition. G.M.: conceptualization, resources, supervision, project administration, and funding acquisition. All authors have read and agreed to the published version of the manuscript.

Notes

The authors declare no competing financial interest.

ACKNOWLEDGMENTS

This project has received funding from the European Union's Horizon 2020 research and innovation program under Grant Agreement No. 869467 (SEArcularMINE). This output reflects only the author's view. The European Health and Digital Executive Agency (HaDEA) and the European Commission cannot be held responsible for any use that may be made of the information contained therein.

NOMENCLATURE

A active membrane area (m^2)
C molar concentration (mol/L)
C^c concentrated solution (mol/L)
C^d diluted solution (mol/L)
$C^m_{Co\text{-}ion}$ co-ions in the membrane (mol/kg)
$C^m_{Counter\text{-}ion}$ counterions in the membrane (mol/kg)
C^m_{fix} membrane fixed charge (mol/kg)
I electric current (I)
Mg-CGCR magnesium hydroxide crystallization reactor
M_{sol} volume of desorption solution
MW_i molar weight of the ion
N number of cell pairs (-)
OCV open circuit voltage (V)
P power (W)
P_d power density (W/m^2 cell pair)
$P_{d\,corr}$ corrected power density (W/m^2 cell pair)
R_{blank} blank resistance (Ω)
R_{cell} resistance of cell pair (Ω)
R_{stack} stack internal resistance (Ω)
R_{load} load resistance
V_{stack} stack potential (V)
T temperature (K)
v fluid flow velocity (cm/s)
α permselectivity
z_i ion valance number
AEM anion exchange membrane
CEM cation exchange membrane
ERS electrode rinse solution
IEM sion exchange membrane
HC high compartment
LC low compartment
RED reverse electrodialysis
SGP sanity gradient power

REFERENCES

(1) International energy outlook 2013. 2013. https://www.eia.gov/outlooks/ieo/pdf/0484(2013).pdf (accessed Oct 17, 2022).

(2) Pattle, R. E. Production of Electric Power by mixing Fresh and Salt Water in the Hydroelectric Pile. *Nature* **1954**, *174* (4431), 660.

(3) Avci, A. H.; Tufa, R. A.; Fontananova, E.; Di Profio, G.; Curcio, E. Reverse Electrodialysis for energy production from natural river water and seawater. *Energy* **2018**, *165*, 512−521.

(4) Hu, J.; Xu, S.; Wu, X.; Wang, S.; Zhang, X.; Yang, S.; Xi, R.; Wu, D.; Xu, L. Experimental investigation on the performance of series control multi-stage reverse electrodialysis. *Energy Convers. Manage.* **2020**, *204*, No. 112284.

(5) Shah, S. A.; Choi, S. Y.; Cho, S.; Shahbabaei, M.; Singh, R.; Kim, D. Modified single-wall carbon nanotube for reducing fouling in perfluorinated membrane-based reverse electrodialysis. *Int. J. Hydrogen Energy* **2020**, *45* (55), 30703−30719.

(6) Vermaas, D. A.; Saakes, M.; Nijmeijer, K. Doubled power density from salinity gradients at reduced intermembrane distance. *Environ. Sci. Technol.* **2011**, *45* (16), 7089.

(7) Sharma, P. P.; Singh, R.; Shah, S. A.; Yoo, C. H.; Lee, A. S.; Kim, D.; Na, J. G.; Lee, J. S. Strategically Altered Fluorinated Polymer at Nanoscale for Enhancing Proton Conduction and Power Generation from Salinity Gradient. *Membranes* **2022**, *12* (4), 395.

(8) Turek, M.; Bandura, B.; Dydo, P. Power production from coal-mine brine utilizing reversed electrodialysis. *Desalination* **2008**, *221* (1−3), 462−466.

(9) Tedesco, M.; Scalici, C.; Vaccari, D.; Cipollina, A.; Tamburini, A.; Micale, G. Performance of the first reverse electrodialysis pilot plant for power production from saline waters and concentrated brines. *J. Membr. Sci.* **2016**, *500*, 33−45.

(10) Tufa, R. A.; Curcio, E.; Brauns, E.; van Baak, W.; Fontananova, E.; di Profio, G. Membrane Distillation and Reverse Electrodialysis for Near-Zero Liquid Discharge and low energy seawater desalination. *J. Membr. Sci.* **2015**, *496*, 325−333.

(11) Tufa, R. A.; Rugiero, E.; Chanda, D.; Hnat, J.; Baak, W. V.; Veerman, J.; Fontananova, E.; di Profio, G.; Drioli, E.; Bouzek, K.; Curcio, E. Salinity gradient power-reverse electrodialysis and alkaline polymer electrolyte water electrolysis for hydrogen production. *J. Membr. Sci.* **2016**, *514*, 155−164.

(12) Emdadi, A.; Gikas, P.; Farazaki, M.; Emami, Y. Salinity gradient energy potential at the hyper saline Urmia Lake − ZarrinehRud River system in Iran. *Renewable Energy* **2016**, *86*, 154−162.

(13) Abdullah Shah, S.; Haider, Z.; Shahbabaei, M.; Kim, D. Development of an Efficient System for Blue Energy Production

Based on Reverse Electrodialysis (RED) by Optimizing Electrolyte Composition: Experimental and Theoretical Simulations. *Energy Fuels* **2022**, *36*, 6353.
(14) Loeb, S.; Norman, R. S. Osmotic Power Plants. *Science* **1975**, *189* (4203), 654−655.
(15) Tufa, R. A.; Curcio, E.; Fontananova, E.; Di Profio, G. 3.8 Membrane-Based Processes for Sustainable Power Generation Using Water: Pressure-Retarded Osmosis (PRO), Reverse Electrodialysis (RED), and Capacitive Mixing (CAPMIX). In *Comprehensive Membrane Science and Engineering*; Elsevier, 2017; pp 206−248 DOI: 10.1016/B978-0-12-409547-2.12278-4.
(16) Sales, B. B.; Saakes, M.; Post, J. W.; Buisman, C. J. N.; Biesheuvel, P. M.; Hamelers, H. V. M. Direct Power Production from a Water Salinity Difference in a Membrane-Modified Supercapacitor Flow Cell. *Environ. Sci. Technol.* **2010**, *44* (14), 5661−5665.
(17) Olsson, M.; Wick, G. L.; Isaacs, J. D. Salinity Gradient Power: Utilizing Vapor Pressure Differences. *Science* **1979**, *206* (4417), 452−454.
(18) Vassallo, F.; La Corta, D.; Cancilla, N.; Tamburini, A.; Bevacqua, M.; Cipollina, A.; Micale, G. A pilot-plant for the selective recovery of magnesium and calcium from waste brines. *Desalination* **2021**, *517*, No. 115231.
(19) Consortium - SEArcularMine. 2022. https://searcularmine.eu/about/consortium/ (accessed Sep 21, 2021).
(20) Veerman, J.; Saakes, M.; Metz, S. J.; Harmsen, G. J. Reverse electrodialysis: Performance of a stack with 50 cells on the mixing of sea and river water. *J. Membr. Sci.* **2009**, *327* (1-2), 136−144.
(21) Daniilidis, A.; Vermaas, D. A.; Herber, R.; Nijmeijer, K. Experimentally obtainable energy from mixing river water, seawater or brines with reverse electrodialysis. *Renewable Energy* **2014**, *64*, 123−131.
(22) Tedesco, M.; Brauns, E.; Cipollina, A.; Micale, G.; Modica, P.; Russo, G.; Helsen, J. Reverse electrodialysis with saline waters and concentrated brines: A laboratory investigation towards technology scale-up. *J. Membr. Sci.* **2015**, *492*, 9−20.
(23) Kim, H.-K.; Lee, M.-S.; Lee, S.-Y.; Choi, Y.-W.; Jeong, N.-J.; Kim, C.-S. High power density of reverse electrodialysis with pore-filling ion exchange membranes and a high-open-area spacer. *J. Mater. Chem. A* **2015**, *3* (31), 16302−16306.
(24) Choi, S.-Y.; Sharma, P. P.; Shah, A.; Singh, R.; Kim, D.; Jin, K.-S. Controlling Fuel Crossover in Open Electrochemical Cells by Tuning the Water Nanochannel for Power Generation. 2020 DOI: 10.1021/acssuschemeng.0c01013.
(25) Guo, Z.-Y.; Ji, Z. Y.; Zhang, Y. G.; et al. Effect of ions (K+, Mg2+, Ca2+ and SO42−) and temperature on energy generation performance of reverse electrodialysis stack. *Electrochim. Acta* **2018**, *290*, 282−290.
(26) Tristán, C.; Fallanza, M.; Ibáñez, R.; Ortiz, I. Reverse Electrodialysis: Potential Reduction in Energy and Emissions of Desalination. *Appl. Sci.* **2020**, *10* (20), 7317.
(27) Simões, C.; Vital, B.; Sleutels, T.; Saakes, M.; Brilman, W. Scaled-up multistage reverse electrodialysis pilot study with natural waters. *Chem. Eng. J.* **2022**, *450*, No. 138412.
(28) Cosenza, A.; Campisi, G.; Giacalone, F.; Randazzo, S.; Cipollina, A.; Tamburini, A.; Micale, G. Power Production from Produced Waters via Reverse Electrodialysis: A Preliminary Assessment. *Energies* **2022**, *15* (11), 4177.
(29) Yasukawa, M.; Mehdizadeh, S.; Sakurada, T.; Abo, T.; Kuno, M.; Higa, M. Power generation performance of a bench-scale reverse electrodialysis stack using wastewater discharged from sewage treatment and seawater reverse osmosis. *Desalination* **2020**, *491*, No. 114449.
(30) https://www.fujifilm.com/us/en/business/industrial-materials/ion-exchange-membranes/overview (accessed March 23, 2024).
(31) https://www.watertechnologies.com/products/ionics-ion-exchange-membranes (accessed March 23, 2024).
(32) Pitzer, K. S. *Activity Coefficients in Electrolyte Solutions*; CRC Press, 1991.
(33) Abdullah Shah, S.; Cucchiara, R.; Vicari, F.; Cipollina, A.; Tamburini, A.; Micale, G. Energetic Valorisation of Saltworks Bitterns via Reverse Electrodialysis: A Laboratory Experimental Campaign. *Membranes* **2023**, *13* (3), 293.
(34) Donnan, F. G. The Theory of Membrane Equilibria. *Chem. Rev.* **1924**, *1* (1), 73−90.
(35) Galizia, M.; Manning, G. S.; Paul, D. R.; Freeman, B. D. Ion partitioning between brines and ion exchange polymers. *Polymer* **2019**, *165*, 91−100.
(36) Ersöz, M.; Güğül, İlkay Hilal.; Çimen, Aysel.; Leylek, Betül.; Yildiz, Salih.; Ers, M.; Leylek, B.; Yildiz, S. The Sorption of Metals on the Polysulfone Cation Exchange Membranes. https://journal-s.tubitak.gov.tr/chem: https://journals.tubitak.gov.tr/chem/vol25/iss1/5.
(37) Zlotorowicz, A.; Strand, R. V.; Burheim, O. S.; Wilhelmsen, Ø.; Kjelstrup, S. The permselectivity and water transference number of ion exchange membranes in reverse electrodialysis. *J. Membr. Sci.* **2017**, *523*, 402−408.
(38) Weinstein, J. N.; Leitz, F. B. Electric Power from Differences in Salinity: The Dialytic Battery. *Science* **1976**, *191* (4227), 557−559.
(39) Hong, J. G.; Gao, H.; Gan, L.; Tong, X.; Xiao, C.; Lui, S.; Zhang, B.; Chen, Y. Nanocomposite and nanostructured ion-exchange membrane in salinity gradient power generation using reverse electrodialysis. In *Advanced Nanomaterials for Membrane Synthesis and its Applications*; Elsevier, 2019; pp 295−316 DOI: 10.1016/B978-0-12-814503-6.00013-6.
(40) Gurreri, L.; Tamburini, A.; Cipollina, A.; Micale, G.; Ciofalo, M. CFD prediction of concentration polarization phenomena in spacer-filled channels for reverse electrodialysis. *J. Membr. Sci.* **2014**, *468*, 133−148.
(41) Vermaas, D. A.; Guler, E.; Saakes, M.; Nijmeijer, K. Theoretical power density from salinity gradients using reverse electrodialysis. *Energy Procedia* **2012**, *20*, 170−184.
(42) Gurreri, L.; Tamburini, A.; Cipollina, A.; Micale, G.; Ciofalo, M. Flow and mass transfer in spacer-filled channels for reverse electrodialysis: a CFD parametrical study. *J. Membr. Sci.* **2016**, *497*, 300−317.

https://doi.org/10.1021/acsomega.4c08651
ACS Omega 2025, 10, 29980−29991